

Flexible, Large-Area Covert Polarization Display Based on Ultrathin Lossy Nanocolumns on a Metal Film

Joo Hwan Ko, Young Jin Yoo, Yeong Jae Kim, Sang-Shin Lee, and Young Min Song*

Covert polarization displays provide a barrier to the inadvertent viewing of stored optical information. For security and anti-counterfeiting purposes, access to concealed information without compromising packaging aesthetics is required in certain situations. However, optical conversion with polarized light typically requires sophisticated nanostructures only possible with limited materials, which are not appropriate for application to objects requiring flexibility or conformability, and color selectivity. A flexible, large-area covert polarization display based on ultrathin lossy nanocolumns with wide color selectivity is presented. Self-aligned porous nanocolumns (PNCs) fabricated by glancing angle deposition are a facile approach to polarization distinguishable structures. PNCs deposited on metal are designed to switch color in accordance with polarization by ultrathin resonance, which is modeled using the complex effective refractive index. Several combinations of material and thickness are presented to extend color selectivity with the standard red green blue gamut and color palette. As a demonstration, covert polarization display labels are attached to daily objects with curved and wrinkled surfaces, and hidden quick response codes are revealed by polarization adjustment in indoor and outdoor environments. Moreover, a multifunctional water contact detection covert polarization display is demonstrated based on the sensitivity of PNCs to the refractive index of the analyte.

1. Introduction

Recently developed concepts in structural color open up opportunities for future applications including nanocolor painting,^[1–7] chiral reflectors/filters,^[8–10] and digital micro-displays.^[11–14] Together with these possibilities, compared to conventional dyes/pigments, structural colors have improved potential for fine-tunability of color achieved by controlling their dimensions, as well as for sustainable production, and

durability. Each of these capabilities also facilitates the creation of security features for anti-counterfeiting. Some of the most successful demonstrations of structural color involve 3D chiral color prints,^[8–10] surface plasmon-mediated optical recording,^[13] covert images from plasmonic cavities,^[11,14] etc. Printed/engraved images or codes using such specialized optical media can only be retrieved if the physical structure in every zone is completely known a priori.


Since most of these methods use dielectric/metallic nanostructures that resonate at a particular wavelength or for a particular polarization of light, in order to improve the optical performance, much attention has recently been paid to geometrical optimization and/or material selection.^[5–8,12–15] The reported experimental demonstrations are mainly achieved by elaborate processes (using e-beam lithography or focused ion beam lithography) to define arrays of nanopatterns, however, practical use of such processes is restricted to overall lateral dimensions of less than a few millimeters. For realistic applications occur-

ring in many aspects of daily life (including quick response (QR) codes, banknotes, identity cards, medicine, and consumer goods), cost, throughput, areal coverage, and flexibility/conformability are important considerations.^[16–20] Angular robustness is also one of the key factors for the successful recognition of encrypted information printed on curved or complex surfaces.^[21,22] Achieving all of these features in a single photonic architecture is challenging.

Herein, we present a covert polarization display to break through the flexibility/scalability limitation by using ultrathin lossy nanocolumns deposited on a metal film. Color optical data labels are selectively recognized depending on polarization. For practicality with familiar everyday objects, our designs are demonstrated to exhibit angular independency when applied to various shapes of objects (i.e., a bottleneck, snack bag, and food container). Moreover, multifunctional covert polarization displays with water contact detection are designed based on the external refractive index sensitivity of porous nanocolumns (PNCs). In the fabrication process, we conducted a fabrication test of a design with a wide scale ranging from small to large. From the fabricated sample, optical/color measurements were performed over the entire area with a linear polarizer employed

J. H. Ko, Y. J. Yoo, Y. J. Kim, Prof. Y. M. Song
School of Electrical Engineering and Computer Science
Gwangju Institute of Science and Technology
Gwangju 61005, Republic of Korea
E-mail: ymsong@gist.ac.kr

Prof. S.-S. Lee
Department of Electronic Engineering
Kwangju University
Seoul 01897, Republic of Korea

 The ORCID identification number(s) for the author(s) of this article can be found under <https://doi.org/10.1002/adfm.201908592>.

DOI: 10.1002/adfm.201908592

as an analyzer. For color switching, we optimize the structural design and material selection of PNCs. Furthermore, considering various material combinations, rigorous coupled-wave analysis (RCWA) is performed to demonstrate switchable color sets of extended color range in polarized light.^[23]

2. Results and Discussion

2.1. Basic Concept of Covert Polarization Display with Ultrathin Lossy Nanocolumns

Figure 1a illustrates a schematic of a polarization switchable display using ultrathin lossy nanocolumns aligned by glancing angle deposition (GLAD). The ultrathin resonator consists of PNCs deposited on a metal film. The proposed color display

is composed of PNCs with local orientations varied by GLAD corresponding to each patterned area (**Figure 1a** upper-right). This difference in plane orientation causes a structural color change of the PNC on the metal film depending on the polarization angle (**Figure 1a** bottom-right). The polarization display comprises selected material combinations of PNCs and metals serving as partial and full reflectors. Representatively, we demonstrate these concepts using a combination of germanium (Ge) as PNCs and gold (Au) as a metal reflector. Using the color variation of the PNCs, a polarization switchable display with letter patterns was designed to have a uniform color in unpolarized light (i.e., to the naked eye) and different colors for each polarization (i.e., s-polarization and p-polarization) (**Figure 1b**; **Movie S1**, Supporting Information). For structural details, the corresponding cross-sectional schematic and thickness information are offered in **Figure S1** in the Supporting Information.

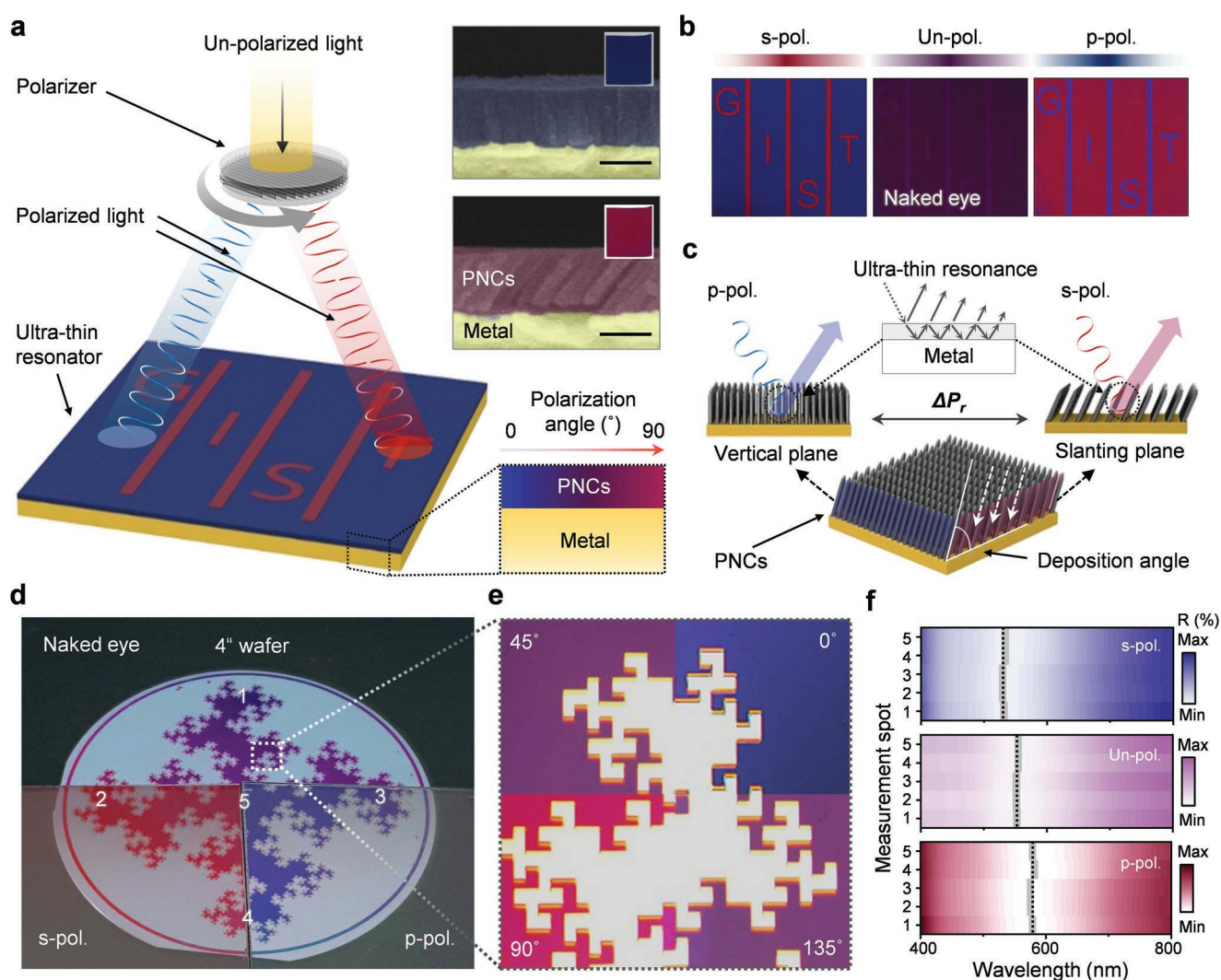


Figure 1. a) Schematic illustration of a polarization switchable display using ultrathin lossy nanocolumns aligned by glancing angle deposition (GLAD). b) Color images of polarization switchable display for each polarization (s-polarization, unpolarized, and p-polarization). c) Schematic of color switching mechanism of porous nanocolumns (PNCs) for different views of in-plane orientation. d) Large-area fractal pattern of PNCs on 4 in. wafer with polarizers aligned to different angles. e) Optical micrograph of smallest fractal patterns (20 μm) for different polarization angles (0°, 45°, 90°, and 135°). f) Measured reflectance spectra with resonant dips (dashed lines) at different measurement positions for each polarization (s-polarization, unpolarized, and p-polarization) for uniformity test. The measurement positions are numbered in five places on the sample image in (d).

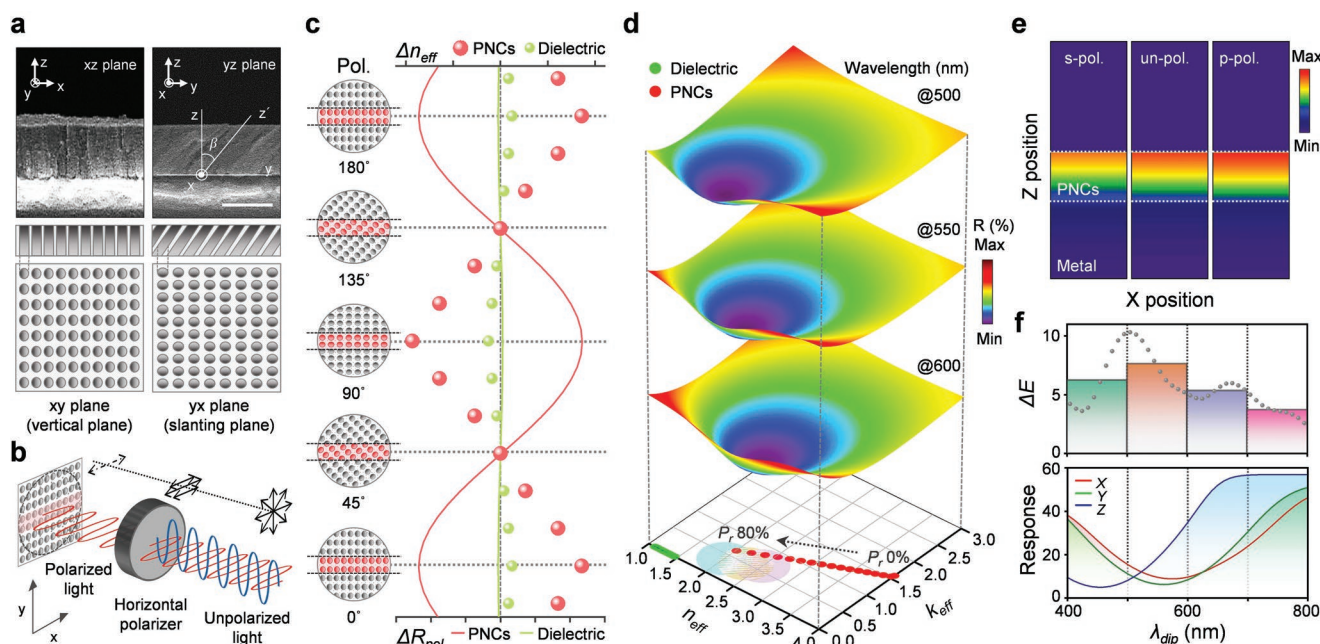


Figure 2. a) Cross-sectional SEM images of PNCs with schematic views of side (xz-plane and yz-plane) and top (xy-plane and yx-plane) depending on plane orientations. b) Schematic illustration of different effective media of PNCs for each polarization. c) Comparison of changes in effective refractive index and reflectance with respect to polarization angles of a highly lossy material (Ge) and a conventional dielectric (SiO₂) at 600 nm. d) Stacked contour plots of reflectance for an ultrathin resonant layer ($t = 35$ nm) on metal (Au) for several wavelengths (500, 550, and 600 nm) versus the complex effective refractive index (n_{eff} and k_{eff}), together with the changes in complex effective refractive index depending on P_r of the highly lossy material and the dielectric material. e) Absorption intensity distributions of PNCs with the highly lossy material in each polarization at 600 nm. f) Color difference and spectral response of tristimulus function with respect to the reflective dip position in the visible wavelengths.

To visualize the color switching mechanism, Figure 1c shows a schematic of different views of in-plane orientations of PNCs. Slanted PNCs were formed by tilting the substrate with respect to the direction of the incoming vapor at a specific deposition angle. In the view of the slanting plane, due to the atomic shadowing effect during GLAD, the PNCs have a relatively higher porosity (P_r) than that in the view of the vertical plane.^[24] Combining PNCs and metals give access to strong resonant behavior much thinner than the wavelength of light led by concomitant nontrivial interface phase shifts.^[1] Therefore, the color variation associated with the difference in ultrathin resonance conditions arises from different effective media with change in P_r of PNCs for each polarization.

To demonstrate scalability, we fabricated a large-area sample of a fractal design including patterns from the micrometer (μm) scale to the centimeter (cm) scale (Figure 1d; Movies S2 and S3, Supporting Information). PNCs can be patterned down to a few-micrometer-size, generally known as resolution limit of conventional lithography techniques (see Figure S2 in the Supporting Information for the result of the lithography test). When observed with polarizers aligned to different optical axes, the fabricated fractal pattern exhibits different colors for each area of the pattern. As shown in the micrographs, the color sensitivity was confirmed at each polarization angle even in the small-scale pattern (i.e., $20 \mu\text{m}$) of the fabricated sample (Figure 1e). Furthermore, the large-area sample shows excellent uniformity over the whole area in the same position as the reflection dip, at various measurement positions, and exhibits different colors for each polarization (Figure 1f).

2.2. Structural Design and Material Selection for Color Switching

As a simple and effective structural approach for color switching, we employed unidirectional slanted PNCs. Figure 2a presents cross-sectional scanning electron microscopy (SEM) images with schematic views for plane orientations of PNCs (i.e., xz-plane and yz-plane), and schematic top views (i.e., xy-plane and yx-plane). The unidirectional slanted PNCs were formed by atomic shadowing depending on the deposition angle, which created wider voids between the sloped columns in the view of the slanting plane.^[24–27] These differences in the arrangement space of the nanocolumns with plane orientations can be considered as different effective media in each polarization of light (Figure 2b).^[28,29]

For consideration of favorable materials for color conversion with PNCs, Figure 2c depicts a comparison of changes in the effective refractive index and reflectance with respect to the polarization angle for a highly lossy material (Ge) and a conventional dielectric (SiO₂). For quantitative comparison, it is assumed that the highly lossy material and the dielectric material have the same porous geometry based on the volume averaging theory (VAT),^[30] and calculation of the effective refractive index and corresponding reflectance as a function of polarization angle is performed (see Figure S3 in the Supporting Information for details). The results show that the highly lossy material exhibits a drastic change in effective refractive index and reflectance relative to that of the dielectric material as a function of polarization angle at a specific visible wavelength

(i.e., 600 nm) (see Figures S4 and S5 in the Supporting Information for details).

For optimization of P_r in color spectral range, Figure 2d shows stacked contour plots of the reflectance at several wavelengths (i.e., 500, 550, and 600 nm) versus the complex effective refractive index (i.e., n_{eff} and k_{eff}). The changes in complex effective refractive index depending on P_r of the highly lossy material and the dielectric material are also shown. To perform optical calculations, we designed an ultrathin resonant layer ($t = 35$ nm) on metal (Au), and applied materials with different complex effective refractive indices to the resonant layer. In the calculated reflectance contours, resonant dips were observed at each wavelength, and by projecting the resonant areas onto the plane, we noted that the resonance regions tend to shift on the complex refractive index plane for swept wavelengths. Accordingly, in the complex effective refractive index change with P_r , the highly lossy material satisfies the resonance optimum range and coincides with P_r modulation range for the polarization angle variation. As an intuitive illustration of resonance, the absorption intensities of PNCs with the highly lossy material for each polarization at a specific wavelength (600 nm) were calculated (Figure 2e). The result shows that strong absorption occurs due to resonance in the PNC layer, and absorption intensity distributions vary for each wavelength.

The change in polarization dependent reflectivity for visible light enables PNC color switching. Thus, to analyze the chromatic response for reflective polarization display applications, we considered the color difference and the spectral response of the tristimulus function with respect to the reflective dip position at visible wavelengths (Figure 2f).^[31] For reflective spectra following the subtractive color scheme, we modeled a spectral

curve with a minimum dip using a Gaussian distribution and calculated chromatic values by sweeping the dip position over visible wavelengths (Figure S6, Supporting Information). As a result, the Z value of the tristimulus function rapidly changes over the range 500–600 nm, and correspondingly, the color difference (ΔE) shows the highest average variation over the same range. From this result, it is noted that our PNC design is favorable for color switching with the corresponding resonant wavelength range in the polarization variation.

2.3. Material Combinations for Color Selectivity and Experimental Confirmation

For color selectivity of the polarization switchable display with the optimized PNCs, chromatic values were converted from calculated reflectances of various combinations of highly lossy materials. Figure 3a displays the results for both polarized and unpolarized light of chromaticity plots for the standard red green blue (sRGB) gamut (white line) on CIE coordinates. In unpolarized light, even with several material/thickness combinations, the results show a relatively confined area of chromaticity within the sRGB gamut. However, for polarized light, depending on the polarization angle, the color range of the combinations is extended toward and even outside the boundary of the sRGB gamut. For total color representation of the combinations, Figure 3b presents a color palette with different polarization angles (see Figure S7 in the Supporting Information for details). Furthermore, as mentioned in Figure 2f, some combinations of PNCs with dip modulation in the wavelength range of 500–600 nm for polarization variation

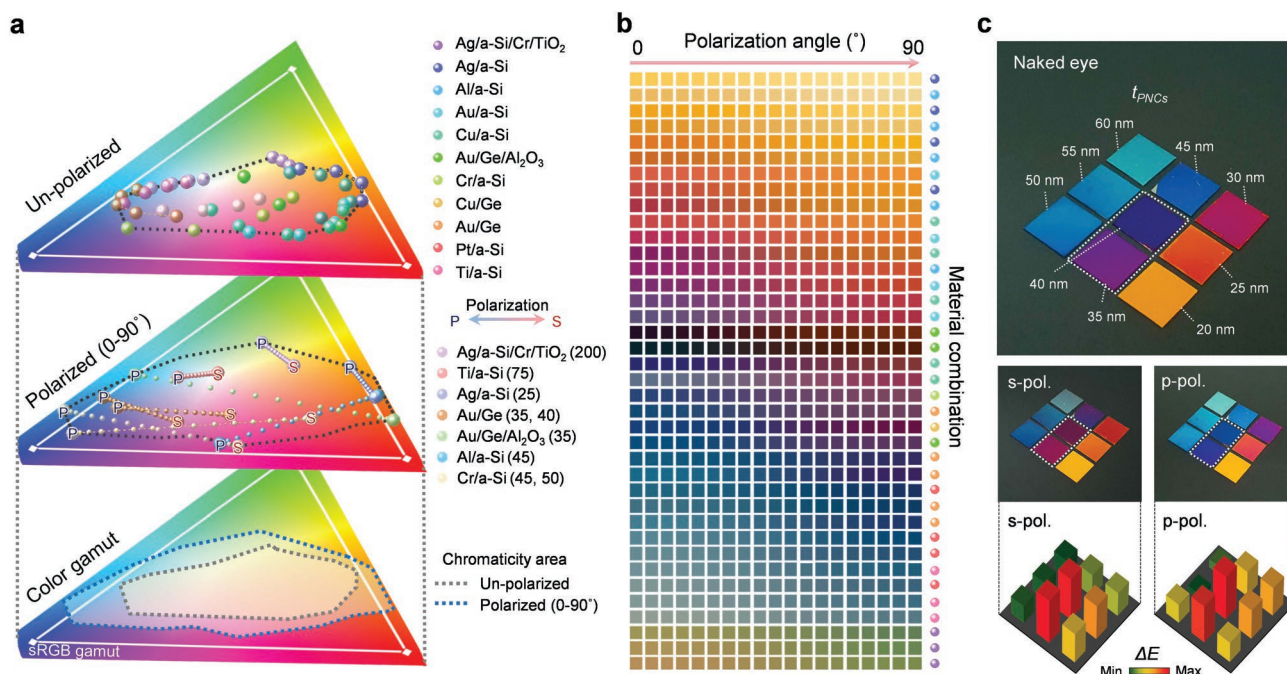


Figure 3. a) Chromaticity plots for sRGB gamut (white line) on CIE coordinates for several material and thickness combinations in unpolarized and polarized light. b) Color palette of several material and thickness combinations for different polarization angles. c) Fabricated sample images of PNCs (Au/Ge) with different thicknesses (20–60 nm) in each polarization and the color difference (ΔE) of the samples for the naked eye (i.e., unpolarized light), and for s- and p-polarizations.

show drastic color switching. Color differences are dependent on the spectral response due to the material/thickness combination (see Figure S8 in the Supporting information for details). Especially, for color differences estimated by Euclidean distance (ΔE), specific combinations exhibit higher values of 75 or more, depending on the polarization change (Figure S9, Supporting Information). By calculating various material/thickness combinations to confirm the universality of our scheme, we note that the polarization can be an additional means to modulate color without structural modification in ultrathin coloration.

For experimental implementation and as a representative combination of PNCs, we fabricated several samples with different thicknesses (20–60 nm) of Au/Ge combinations. As a verification of the results, we conducted optical measurements and color evaluations on all fabricated samples. Measurement data including reflectance spectra, CIE coordinate plots, and color representation for each sample are shown in Figure S10 in the Supporting Information. In addition, compared with the calculated reflection spectra, the fabricated samples show that the dip position is well matched to the calculation results for different polarization angles (Figure S11, Supporting Information). Figure 3c shows a fabricated sample image for each polarization, and the color difference (ΔE) of the samples for the s- and p-polarizations for the naked eye (i.e., unpolarized light). As expected from these results, 35 and 40 nm thick samples (enclosed by white-dashed lines) with dip modulation

in the wavelength range around 500–600 nm show the highest color differences in each polarization.

2.4. Covert Display Demonstration with Flexibility

As a practical application, exploiting the flexibility and polarization sensitivity of PNCs, Figure 4a illustrates a schematic of covert polarization display including optical data (e.g., QR code) with a series of processes of the QR code authentication. The covert display is hidden in the observation environment of the naked eye (i.e., unpolarized light), while the stored QR code on the covert display is visible by rotating an analyzer (i.e., linear polarizer) to a predetermined polarization angle. Furthermore, the QR code can be used to authenticate the operator of a smartphone (Movie S4, Supporting Information). For flexibility/conformability to various objects and/or surfaces, we fabricated a polarization covert display on a polyester thin-film ($t = 2.5 \mu\text{m}$) as shown in Figure 4b. The fabricated sample was observed to be an almost uniform color with a rarely visible pattern in unpolarized light (Figure 4c left), and the QR code on the sample was clearly revealed in a different color in polarized light (Figure 4c right). The covert display in hidden mode (unpolarized light) has a low contrast of 6.49%, and in visible mode has a contrast of 61.68%, which exceeds the QR code authentication requirement of 40% contrast (Figure 4d; see Figure S12 in the Supporting Information for details).

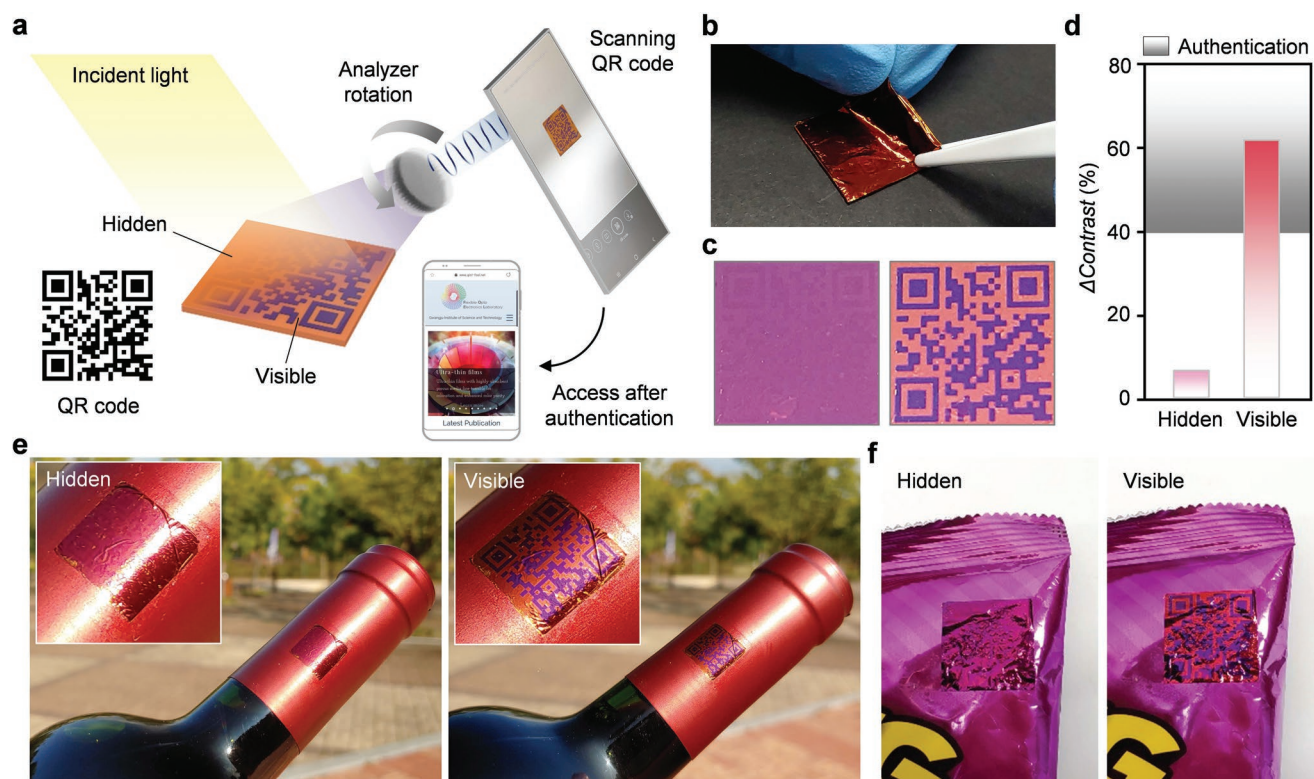


Figure 4. a) Schematic illustration of covert polarization display including optical data (QR code) and series of processes for QR code authentication. b) Fabricated sample of polarization covert display on a polyester thin-film ($t = 2.5 \mu\text{m}$). c) Sample images of covert polarization display in hidden and visible modes. d) Measured contrast values of covert polarization display in hidden and visible modes. e) Covert display label on a curved surface of a wine bottle in outdoor environment. f) Covert display label on the wrinkled surface of a snack bag in an indoor environment.

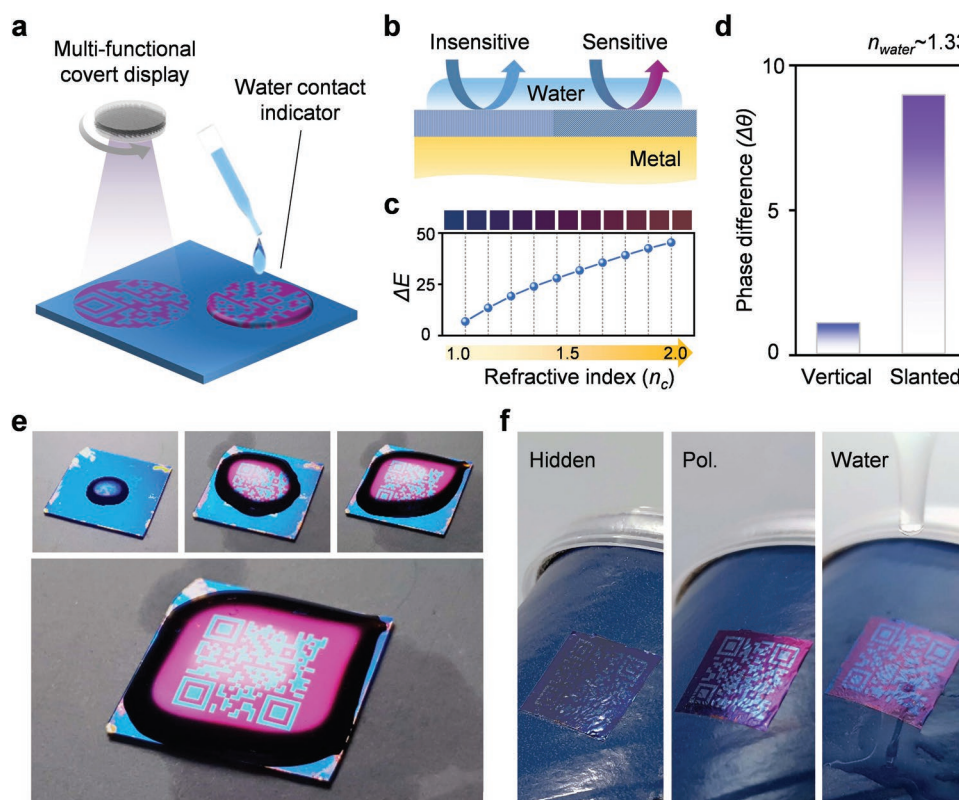


Figure 5. a) Schematic of multifunctional covert polarization display as water contact indicator. b) Cross-sectional schematic views of divided areas insensitive to and sensitive to water by forming vertical and slanted nanocolumns at different deposition angles (0° and 70°). c) Color difference (ΔE) with external refractive index change of the PNC designed for sensitive areas. d) Phase difference ($\Delta\theta$) at the interface with water in sensitive (slanted) and insensitive (vertical) areas. e) Water contact images of multifunctional covert display with water gradually dropped onto the surface. f) Multifunctional covert display label on a curved food container with different observation modes (hidden, polarization, and water).

For demonstration of application to commercial products, we applied covert display labels to a wine bottleneck with a curved surface (Figure 4e) and a snack bag with a wrinkled surface (Figure 4f). In hidden mode with the naked eye (i.e., unpolarized light), the covert display label is similar to the color of the product, and does not spoil the aesthetics of the product design. However, when authentication is required, the covert display label in visible mode in polarized light reveals the stored QR code in outdoor and indoor environments. As presented above in Figure 3b, the polarization covert display is advantageous because it can be designed to match the target product color because of its wide color selectivity. Moreover, the covert display exhibits angular robustness because it is based on ultrathin resonance (see Figure S13 in the Supporting Information for calculation and measurement results on angular characteristics), which increases the success rate of QR code recognition even on curved and wrinkled surfaces (Movie S5, Supporting Information).

In addition, the versatile selectivity of the polarization display allows a wide range of color switching applications. Multistate color designs can be created by combining material and thickness selection, with alignment direction of PNCs using conventional lithographic techniques. As simple examples, using the polarization display with PNCs, we fabricated samples of multiple optical data storage labels through pixel

combinations and several simple patterns inserted into one image (Figure S14, Supporting Information).

2.5. Multifunctional Covert Polarization Display Label for Water Contact Detection

Figure 5a presents a multifunctional covert polarization display function as a water contact indicator. Due to the low complex effective refractive index with P_r , PNCs are sensitive to subtle external refractive index changes, such as water, on the surface of PNCs (see Figure S15 in the Supporting Information for details). With the sensitivity of PNCs to changes in external refractive index, we designed a covert display divided into areas insensitive to and sensitive to water by forming vertical and slanted nanocolumns at different deposition angles (0° and 70°), respectively (Figure 5b; see Figure S16 in the Supporting Information for details). The PNCs designed for sensitive areas show a distinct change in color difference (ΔE) depending on refractive index changes (Figure 5c). Therefore, when water comes into contact with the surface of the insensitive area, the phase difference rarely occurs in the reflection coefficient at the interface between the covert display and the water due to the high complex refractive index of the highly lossy material, while in the sensitive area, when water comes into contact with the surface, a relatively high phase difference occurs at the

interface with the water due to the low complex refractive index and P_r (Figure 5d). As a result, in the insensitive area, no color change occurs as a result of wetting with water, but in the sensitive area, the color changes due to the resonance condition modulated by the phase difference, thereby revealing the stored optical information (QR code).

Figure 5e shows a fabricated sample of a multifunctional covert polarization display with water contact indicator. The results show that the QR code was partially revealed only in the water contact area as the water was gradually dropped, and when the water covered the whole area, the entire QR code is revealed, which can be authenticated using a smartphone (Movie S6, Supporting Information). As a basic function of the multifunction covert display, the QR code can be revealed even with polarized light (Figure S17, Supporting Information). For realistic application with multifunctionality, we applied a multifunctional covert display label to a round container of food vulnerable to moisture (Figure 5f). Observed by the naked eye, the covert label was hidden in harmony with the food packaging design. The QR code stored for authentication was revealed in polarized light (Movie S7, Supporting Information). When in contact with water, the covert label changed to a different color as a function of the water contact indicator.

3. Conclusion

In conclusion, we presented a clever strategy for switching covert optical information using polarization-dependent multicolors without structurally sophisticated fabrication processes. Depending on the in-plane orientation, the unidirectional slanted PNCs exhibited different P_r , causing ultrathin resonance changes resulting from effective refractive index differences. We verified the universality of this method for different combinations of highly lossy materials, and for several combinations chromaticity extensions with their color palettes were presented. In addition, a large-area sample with a fractal pattern fabricated to verify fabrication scalability exhibited stable uniformity across the entire area. For practical applications, flexible covert display labels with QR codes suggested the convergence of polarization sensitivity and shape deformability of PNCs. A multifunctional covert polarization display label for water contact detection extends the capabilities beyond optical information storage. Moreover, the angular robustness of these ultrathin covert images will enable application in harsh recognition and authentication environments. Given the versatility and extensibility of PNCs, the proposed polarization display is a simple and powerful means for polarization detection and encrypted optical authentication.

4. Experimental Section

Optical Calculation: The RCWA was used to calculate the reflectance of the polarization display with PNCs by using commercial software (DiffractionMOD, RSoft Design Group, USA). The second diffraction order and 0.2 nm grid size were used in the RCWA to calculate the diffraction efficiency, which was sufficient to numerically stabilize the

results. Material dispersions and extinction coefficients were considered for obtaining exact outputs. The commercial software MATLAB (Mathworks, Inc.) was also used to calculate both the effective complex refractive indices based on VAT, and the chromatic information from the reflectance.^[23,31]

Optical Characterization: The reflectance spectra of the fabricated samples were measured using a UV-vis-NIR spectrometer (Cary 500, Varian, USA) at a normal angle of incidence with a tungsten-halogen lamp as a source. The angle dependent reflection spectra were obtained using a variable-angle specular reflectance accessory (VARSA). The optical constants and normalized Mueller matrix of PNCs were obtained using a dual rotating compensator ellipsometer (RC2, J.A. Woollam Co., Inc., USA) with a He-Ne laser as a source.

Deposition of Polarization Display with PNCs: PNC polarization displays were fabricated by GLAD to achieve a tilted nanocolumnar structure. For rigid samples, single side polished silicon (100) wafers were generally selected as the substrate, and were treated with buffered oxide etchant for 3 min to remove the native oxide layer. The substrate was next sequentially sonicated for 5 min in acetone, methanol, and deionized (DI) water, respectively. For flexible samples, a commercial 2.5 μm polyester thin-film (SpectroMembrane, Chemplex Industries, Inc., Palm City, USA) was used. For stable deposition, flexible films were attached to a Si substrate. Both the metal (Au) and PNCs (Ge) were deposited by electron beam evaporation (KVE-E2000, Korea Vacuum Tech Ltd, Korea) under high vacuum ($\approx 10^{-6}$ Torr). The Au film was deposited at a rate of $\approx 2 \text{ \AA s}^{-1}$ to a thickness of 100 nm, which is sufficient to form a metal reflector. The Ge layer was deposited on the Au film after mounting the substrate on an inclined sample holder (customized) to targeted thickness at a rate of $\approx 1 \text{ \AA s}^{-1}$. To ensure uniformity, deposition was performed to half of the target thickness, interrupted, the sample was reloaded upside down over the tilted sample holder (after rotation through 180°), and deposition resumed.^[32] At this point, the tilted sample holder was kept facing the Ge source in the same direction as the first deposition to form unidirectional slanted nanocolumns.

Fabrication of Covert Polarization Display: For patterning the designed area (e.g., letter or QR code) with a selected color to respond differently to each polarization, photolithography was used with an image reversal photoresist (AZ 5214, AZ Electronic Materials, Luxembourg). For the image reversal process, a mask aligner (MJB3 UV400, Karl Suss, Germany) was used with a patterned photomask. In each patterned region, the deposition process described above was repeated in different plane orientations perpendicular to each other. After the deposition process, a lift-off process was used to reveal each patterned area.

Supporting Information

Supporting Information is available from the Wiley Online Library or from the author.

Acknowledgements

J.H.K. and Y.J.Y. contributed equally to this work. This work was supported by the National Research Foundation of Korea (NRF) funded by the Korean government (MSIP) (NRF-2017M3D1A1039288 and NRF-2018R1A4A1025623), and the Korea Institute of Energy Technology Evaluation and Planning (KETEP) and the Ministry of Trade, Industry & Energy (MOTIE) of the Republic of Korea (No. 20183010014310), and Samsung Electronics. Y.J.Y. acknowledges the support from the NRF (NRF-2018H1A2A1060954).

Conflict of Interest

The authors declare no conflict of interest.

Keywords

color switching, covert display, polarization color, porous nanocolumns

Received: October 17, 2019

Revised: December 9, 2019

Published online:

- [1] M. A. Kats, R. Blanchard, P. Genevet, F. Capasso, *Nat. Mater.* **2013**, 12, 20.
- [2] Y. J. Yoo, J. H. Lim, G. J. Lee, K.-I. Jang, Y. M. Song, *Nanoscale* **2017**, 9, 2986.
- [3] G. J. Lee, Y. J. Kim, H. M. Kim, Y. J. Yoo, Y. M. Song, *Adv. Opt. Mater.* **2018**, 6, 1800707.
- [4] C. Liu, Q. Zhang, D. Wang, G. Zhao, X. Cai, L. Li, H. Ding, K. Zhang, H. Wang, D. Kong, L. Yin, L. Liu, G. Zou, L. Zhao, X. Sheng, *Adv. Opt. Mater.* **2018**, 6, 1800146.
- [5] Y. J. Kim, Y. J. Yoo, G. J. Lee, D. E. Yoo, D. W. Lee, V. Siva, H. Song, I. S. Kang, Y. M. Song, *ACS Appl. Mater. Interfaces* **2019**, 11, 11849.
- [6] H. S. Song, G. J. Lee, D. E. Yoo, Y. J. Kim, Y. J. Yoo, D. W. Lee, V. Siva, I. S. Kang, Y. M. Song, *Sci. Rep.* **2019**, 9, 3350.
- [7] B. D. Lucas, J.-S. Kim, C. Chin, L. J. Guo, *Adv. Mater.* **2008**, 20, 1129.
- [8] H. L. Liu, B. Zhang, T. Gao, X. Wu, F. Cui, W. Xu, *Nanoscale* **2019**, 11, 5506.
- [9] W.-J. Chung, J.-W. Oh, K. Kwak, B. Y. Lee, J. Meyer, E. Wang, A. Hexemer, S.-W. Lee, *Nature* **2011**, 478, 364.
- [10] K. E. Shopsowitz, H. Qi, W. Y. Hamad, M. J. MacLachlan, *Nature* **2010**, 468, 422.
- [11] D. Franklin, S. Modak, A. Vázquez-Guardado, A. Safaei, D. Chanda, *Light: Sci. Appl.* **2018**, 7, 93.
- [12] X. M. Goh, Y. Zheng, S. J. Tan, L. Zhang, K. Kumar, C.-W. Qiu, J. K. W. Yang, *Nat. Commun.* **2014**, 5, 5361.
- [13] E. Heydari, J. R. Sperling, S. L. Neale, A. W. Clark, *Adv. Funct. Mater.* **2017**, 27, 1701866.
- [14] E. D. Finlayson, I. R. Hooper, C. R. Lawrence, M. Heath, D. Anderson, J. R. Sambles, P. Vukusic, *Adv. Opt. Mater.* **2018**, 6, 1700843.
- [15] V. I. Belotelov, L. E. Kreilkamp, I. A. Akimov, A. N. Kalish, D. A. Bykov, S. Kasture, V. J. Yallapragada, A. V. Gopal, A. M. Grishin, S. I. Khartsev, M. Nur-E-Alam, M. Vasiliev, L. L. Doskolovich, D. R. Yakovlev, K. Alameh, A. K. Zvezdin, M. Bayer, *Nat. Commun.* **2013**, 4, 2128.
- [16] U. Zschieschang, T. Yamamoto, K. Takimiya, H. Kuwabara, M. Ikeda, T. Sekitani, T. Someya, H. Klauk, *Adv. Mater.* **2011**, 23, 654.
- [17] J. Kim, H. J. Shim, J. Yang, M. K. Choi, D. C. Kim, J. Kim, T. Hyeon, D.-H. Kim, *Adv. Mater.* **2017**, 29, 1700217.
- [18] J.-K. Song, D. Son, J. Kim, Y. J. Yoo, G. J. Lee, L. Wang, M. K. Choi, J. Yang, M. Lee, K. Do, J. H. Koo, N. Lu, J. H. Kim, T. Hyeon, Y. M. Song, D.-H. Kim, *Adv. Funct. Mater.* **2017**, 27, 1605286.
- [19] E. Song, Y. K. Lee, R. Li, J. Li, X. Jin, K. J. Yu, Z. Xie, H. Fang, Y. Zhong, H. Du, J. Zhang, G. Fang, Y. Kim, Y. Yoon, M. A. Alam, Y. Mei, Y. Huang, J. A. Rogers, *Adv. Funct. Mater.* **2018**, 28, 1702284.
- [20] H. Galinski, G. Favraud, H. Dong, J. S. T. Gongora, G. Favaro, M. Döbeli, R. Spolenak, A. Fratalocchi, F. Capasso, *Light: Sci. Appl.* **2017**, 6, e16233.
- [21] K.-T. Lee, S. Seo, J. Y. Lee, L. J. Guo, *Adv. Mater.* **2014**, 26, 6324.
- [22] Y.-K. R. Wu, A. E. Hollowell, C. Zhang, L. J. Guo, *Sci. Rep.* **2013**, 3, 1194.
- [23] M. G. Moharam, E. B. Grann, D. A. Pommet, *J. Opt. Soc. Am. A* **1995**, 12, 1068.
- [24] N. G. Wakefield, J. B. Sörge, M. T. Taschuk, L. W. Bezuidenhout, M. J. Brett, J. C. Sit, *J. Opt. Soc. Am. A* **2011**, 28, 1830.
- [25] M. Losurdo, K. Hingerl, *Ellipsometry at the Nanoscale*, Springer, Berlin, Germany **2013**.
- [26] R. N. Tait, T. Smy, M. J. Brett, *J. Vac. Sci. Technol., A* **1992**, 10, 1518.
- [27] M. M. Hawkeye, M. T. Taschuk, M. J. Brett, *Glancing Angle Deposition of Thin Films: Engineering the Nanoscale*, John Wiley & Sons, Inc., Hoboken, NJ **2014**.
- [28] D. Schmidt, *Ph.D Thesis*, University of Nebraska-Lincoln **2010**.
- [29] D. Schmidt, M. Schubert, *J. Appl. Phys.* **2013**, 114, 083510.
- [30] A. Garahan, L. Pilon, J. Yin, I. Saxena, *J. Appl. Phys.* **2007**, 101, 014320.
- [31] N. Ohta, A. Robertson, *Colorimetry: Fundamentals and Applications*, John Wiley & Sons, Inc., Hoboken, NJ **2006**.
- [32] J. B. Oliver, T. J. Kessler, C. Smith, B. Taylor, V. Gruschow, J. Hettrick, B. Charles, *Opt. Express* **2014**, 22, 23883.